Nanoscale Advances

ROYAL SOCIETY OF CHEMISTRY

PAPER

View Article Online
View Journal | View Issue

Cite this: *Nanoscale Adv.*, 2024, **6**, 3181

Photocatalytic functionalization of thin-layer membranes using a monomer truncation strategy†

Jorge Vega-Fernández, [a] Vanesa Marcos,[ab] Jesús Álvarez, [cdeg] María José Capitán, [fg] Alberto Fraile *[ab] and José Alemán *[ab]

Received 20th February 2024
Accepted 24th April 2024

DOI: 10.1039/d4na00149d

rsc.li/nanoscale-advances

We present the design and synthesis of two new organic polymer films making use of a liquid–liquid interfacial amine–acid chloride polymerization strategy. One of them was additionally functionalized *in situ* by the anchoring of *N*-phenyl-phenothiazine through a monomer truncation strategy, which endowed it with photocatalytic activity. This photoactive film displays interesting luminescence phenomena that were used for the oxidation of a variety of sulphides to their corresponding sulfoxides and reduction of aryl bromines.

Introduction

Within the realm of materials, there exists a special type of expanded organic structure known as two-dimensional polymers.[1] These polymers are typically ordered structures that extend in two orthogonal directions. They have emerged for a variety of reasons, such as the widespread availability of building blocks suitable for their construction and their easy adjustability. The synthesis of extended organic materials has gained significant importance in recent years, especially when these structures can be synthesized as thin films.[2]

One of the best ways to synthesize thin films involves the use of bottom-up interfacial synthesis techniques.[2,3] These techniques have been employed for the synthesis of thin films with various thicknesses, ranging from a few nanometers to hundreds or even a few microns. Different linkers and strategies have been used, with the most common links being imines and boronates, widely utilized in covalent organic frameworks (COFs).[4] Mixtures of liquid–liquid and air–water have been predominantly employed. In this sense, recently, Wang and collaborators prepared a covalent organic network-thin film for molecular separation.[3c] They used a tetraamine and an azo-compound as linkers, creating thin membranes (Scheme 1a).

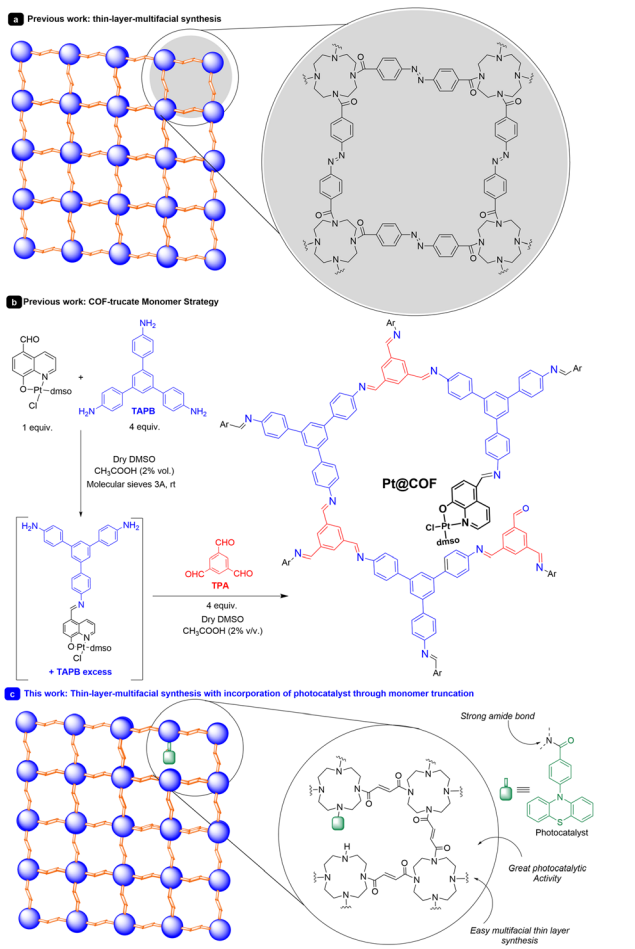

Scheme 1 Previous work in the field and present work.

[a]*Departamento de Química Orgánica (Módulo 1), Facultad de Ciencias, Universidad Autónoma de Madrid, 28049-Madrid, Spain. E-mail: jose.aleman@uam.es; alberto.fraile@uam.es; Web: https://josealemanlara.wixsite.com/froncat*

[b]*Institute for Advanced Research in Chemical Sciences (IAdChem), Universidad Autónoma de Madrid, 28049-Madrid, Spain*

[c]*Departamento de Física de la Materia Condensada, Universidad Autónoma de Madrid, 29049-Madrid, Spain*

[d]*Instituto de Ciencia de Materiales "Nicolás Cabrera", Univ. Autónoma de Madrid, 28049-Madrid, Spain*

[e]*Instituto de Física de la Materia Condensada IFIMAC, Univ. Autónoma de Madrid, 28049-Madrid, Spain*

[f]*Instituto de Estructura de la Materia IEM-CSIC, 28006-Madrid, Spain*

[g]*Física de Sistemas Crecidos con Baja Dimensionalidad, Universidad Autónoma de Madrid, Unidad Asociada al CSIC por el IEM, DP, Madrid, Spain*

† Electronic supplementary information (ESI) available. See DOI: https://doi.org/10.1039/d4na00149d

Despite the synthesis of thin layers with applications in electronics, mechanical properties, sensing, photonics, and molecular transport, the use of these materials in photocatalysis has been more limited.[3b,4,5]

Recently, our research group has described an interesting strategy for incorporating photocatalysts into COF-like structures.[6] This approach, termed the monomer truncation strategy, involves incorporating catalytically active molecular fragments into the COF structure (Scheme 1b). To accomplish this, we manipulated the linking points of a building block. By doing so, we alter one of the functionalities of the building block (in this case one aldehyde), generating structural defects randomly distributed along the COF backbone.[7] In this study, we incorporated a platinum photoredox catalyst to facilitate oxidation reactions.

In this context, it was found that *N*-phenyl-phenothiazine (PTH) is a frequently employed catalyst with excellent reduction potential (E° ($PTH^{\bullet+}$/PTH*) = −2.1 V *vs.* SCE)[8] and good oxidation potential (E° ($PTH^{\bullet+}$/PTH) = 0.68 V *vs.* SCE).[9] In this work, we present, to the best of our knowledge, a novel strategy for incorporating photocatalytic units into thin films through monomer truncation (Scheme 1c). In this process, we have introduced a photocatalyst, in this case, PTH, and applied it to both oxidation and reduction reactions, under practically solvent-free conditions. To achieve this, we have modified the structure of the photocatalyst, which is capable of forming a very robust amide bond.

Results and discussion

Synthesis of the photocatalyst monomer precursor

To prepare the photoactive film **1-PTH**, first it was necessary to synthesise the PTH photocatalytic unit **5**. For that, we followed the synthetic route shown in Scheme 2 which lied in a Buchwald–Hartwig coupling to functionalize the nitrogen atom at the phenothiazine core and, subsequently, the basic hydrolysis of the nitrile group (**4**), obtaining the corresponding carboxylic acid monomer **5** in a 77% overall yield.[10] The spectroscopic data of both intermediates are in agreement with reported data.

Afterwards, to anchor the PTH-photocatalyst unit **5** into the material, the carboxylic group had to be transformed into corresponding acid chloride (**5-Cl**) previously by means of a reaction with thionyl chloride (Scheme 3).

5-Cl was obtained in quantitative yield and used directly, without further purification, to prepare the film materials.

Film preparation and characterization

First, we carried out several trials to find the best conditions to prepare the pristine film **1** without the photocatalytic unit. For

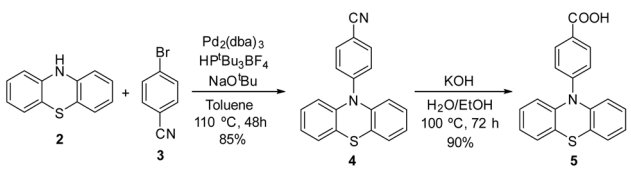

Scheme 2 Synthesis of photocatalyst unit precursor **5**.

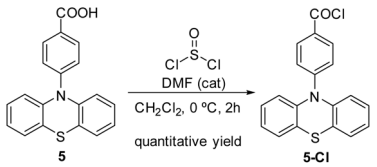

Scheme 3 Synthesis of acid chloride **5-Cl**.

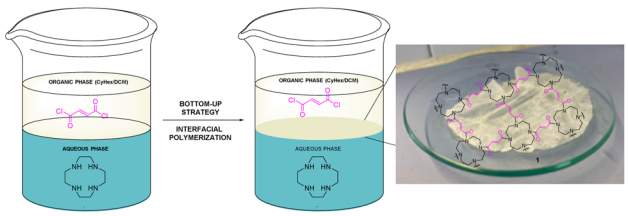

Fig. 1 Synthesis of film **1** by interfacial polymerization.

that, we began studying the condensation between 1,4,7,10-tetraazacyclododecane (cyclen) (**6**), which is very soluble in water, and fumaryl chloride (**7**), both commercially available, making use of the bottom-up strategy in mixtures of water and a non-miscible organic solvent or a combination of two of them (see the ESI† and Fig. 1). The best result was achieved when the organic phase is a 4 : 1 mixture of cyclohexane/dichloromethane which was used after three days at room temperature and the starting of both building blocks (**6** and **7**) in a ratio of 5 : 1, respectively. The film was obtained as a thin white sheet that was very hard-wearing and uniform (see right, Fig. 1).

Once we found the best conditions to prepare the pristine film **1**, we applied those to build the photocatalytic film **1-PTH**. In this case, in the organic phase, in addition to fumaryl chloride, the photoactive monomer **5** was added as the corresponding acid chloride **5-Cl**, previously obtained by treatment of carboxylic acid **5** with thionyl chloride. The use of a 5 : 1 : 1 ratio of **6**, **7** and **5-Cl** allowed the film **1-PTH** to be achieved as a yellow material (Scheme 4).

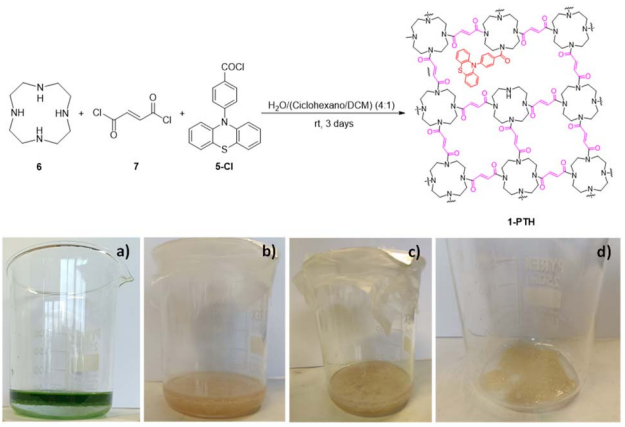

Scheme 4 (Top) Synthesis of photoactive film **1-PTH**. Bottom, pictures of: (a) reaction mixture at zero time; (b) and (c) reaction mixture after 3 days; (d) film after solvent decantation.

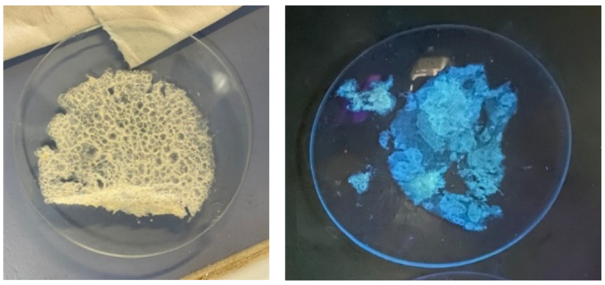

Fig. 2 (Left) Film **1-PTH** obtained. (Right) Film **1-PTH** under UV light (364 nm).

The film shows a structure less compact than that of pristine film **1**, probably due to the defects caused by the random incorporation of the photoactive unit. The presence of the photocatalytic unit in the material structure could be determined by the emission of blue light when it was irradiated under a UV light lamp (364 nm) (Fig. 2, right). Utilizing a reduced amount of the monomer **5-Cl** (0.5 or 0.25 equiv.) resulted in films that lacked light emission when they were irradiated under a UV light lamp (364 nm). Moreover, the maximum emission values were lower than those obtained with film **1-PTH**, which brings to light that the incorporation of monomer **5-Cl** into the material structure was lower (compare Fig. 7d and S8 in the ESI†). For these reasons, we considered that the film **1-PTH**, obtained from the addition of 1.0 equiv. of monomer **5-Cl**, was the most suitable material to be used as the photocatalyst.

Characterization of films

The structures of the prepared films were characterized by means of several techniques. The Fourier-transform infrared spectroscopy (FT-IR) spectra of non-functionalized pristine film **1** show an intense peak at 1630 cm^{-1} corresponding to C=O stretching vibration of the amide group (Fig. 3, red line). Moreover, a broad band between 3640 and 3160 cm^{-1} corresponding to NH or OH stretching vibrations of amine or carboxylic acid groups indicates the presence of both due to the uncomplete condensation of monomers. In addition, two weak peaks at 2923 and 2852 cm^{-1} correspond to C(sp^3)–H stretching vibrations, confirming the presence of a cyclen unit. These same peaks can also be detected in the model structure that belong to *N*,*N*-diethyl-4-(10*H*-phenothiazin-10-yl)benzamide (Fig. 3, blue line).

The functionalized film **1-PTH** (Fig. 3, black line) also shows the same stretching vibration peaks and, additionally, a peak at 1716 cm^{-1}, which could be assigned to the free carboxylic acid derived from fumaryl chloride that may have been due to defects caused by including the photoactive unit. Thus, infrared spectroscopies indicate that both amine and acid chloride building blocks condensed to form an amide-base material.

Successful materials formation can also be determined from the ^{13}C cross-polarization/magic-angle spinning (CP-MAS) solid state NMR spectra of both films (Fig. 4). Thus, both materials (top and middle spectra) show the presence of peaks at around 170, 130 and 49 ppm corresponding to the carbonyl, alkenyl and alkyl carbons, respectively, similarly to the tetraethylfumaramide, which was selected as a model structure (bottom spectra). However, the film **1-PTH** spectrum shows some differences. Thus, the signal at 130 ppm is the most intense and two additional peaks at 144 and 117 ppm can be seen, which can be attributed to the presence of phenyl moieties at the PTH unit.

Thermogravimetric analysis (TGA) for both materials (see the ESI†) indicates that they are thermally stable in air to around 250 °C. Furthermore, the ability to absorb small solvent molecules or water is revealed by a weight loss between 100 and 200 °C. Continuing with the characterization of the materials, both (**1** and **1-PTH**) were analyzed by powder X-ray diffraction, obtaining no crystallinity for either of them. In addition, the gas absorption measurement for the functionalized film **1-PTH** afforded a negligible value (see the ESI†).

The microstructure of the materials was analysed by scanning electron microscopy (SEM). Images of the surface showed a regular and flat structure for film **1** and a laminar but irregular surface for truncated-film **1-PTH** (Fig. 5). A more detailed analysis of the images also indicated that the films obtained are

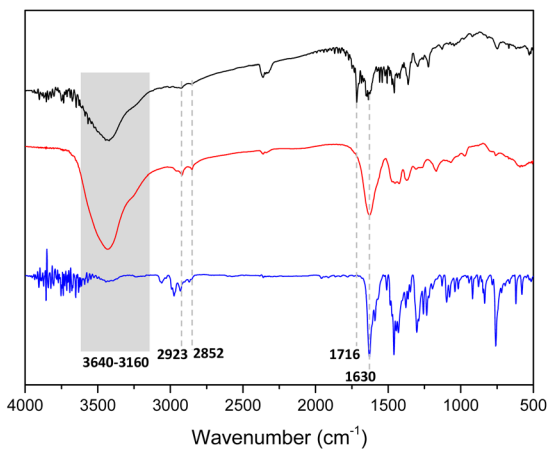

Fig. 3 IR spectra of film **1** (red line), film **1-PTH** (black line) and *N*,*N*-diethyl-4-(10*H*-phenothiazin-10-yl)benzamide (blue line).

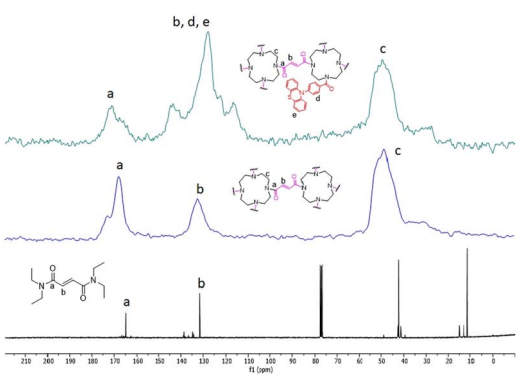

Fig. 4 ^{13}C NMR spectra of film **1-PTH** (top), film **1** (middle) and N^1,N^1,N^4,N^4-tetraethylfumaramide (bottom).

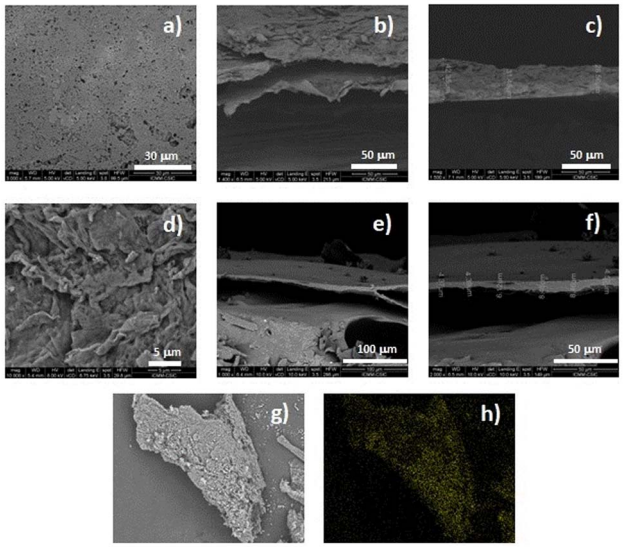

Fig. 5 Top: (a) SEM image and (b) and (c) cross-sectional SEM image for film **1**. Middle: (d) SEM image and (e) and (f) cross-sectional SEM image for film **1-PTH**. Bottom: (g) SEM image and (h) sulphur mapping for film **1-PTH**.

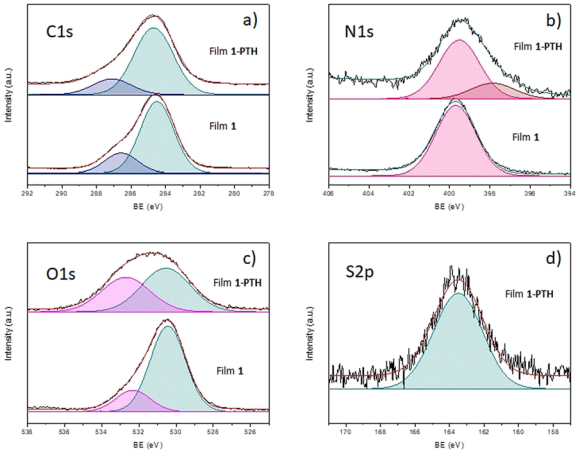

Fig. 6 Results of the photoelectron spectroscopies of film **1** and film **1-PTH**. (a) C1s XPS core level region, (b) N1s XPS core level region, and (c) O1s XPS core level region for both films; (d) S2p XPS core level region of film **1-PTH**.

the result of the stacking of laminar structures (see the ESI†). In addition, the cross-sectional SEM images of the films revealed that the thickness of the layers of functionalized-film **1-PTH** was between 3 and 8.5 microns. However, film **1** is formed by thicker layers (around 30 microns) (Fig. 5 and the ESI†). In conjunction with SEM analysis, energy dispersive X-ray (EDX) analysis was conducted to determine the ratio of functionalization, achieving an average value of 3% by the mass of sulphur (see the ESI†), which indicates that functionalization of around 25% has been reached.

Moreover, EDX analysis revealed the presence of chlorine atoms, which can be explained by the presence of ammonium groups in the material structure due to the protonation of the amino groups of the cyclen unit with the hydrogen chloride released in the condensation reaction of material formation. In addition, the analysis of film **1-PTH** using SEM-EDX mapping (sulphur) showed that functionalization had occurred homogeneously throughout the whole particle (Fig. 5h and the ESI†).

To shed more light on the chemical bonds established in the yielded films, X-ray photoelectron spectroscopy (XPS) analysis was carried out (Fig. 6). Indeed, the survey spectra of both samples presented characteristic XPS C1s (284 eV binding energy (BE)), N1s (399 eV BE) and O1s (530 and 531 eV BE for **1** and **1-PTH**, respectively) core level regions merging out at the survey spectra, while sample **1-PTH** presented an additional peak corresponding to S2p (163.5 eV BE) core level regions as a result of the monomer truncation (see the ESI†). Therefore, this survey analysis cross-checked that the PTH-monomer has been introduced in the structure of the material **1-PTH**. On analyzing the components (Fig. 6), the fit of the XPS C1s core level region afforded two main components for both materials (our equipment did not allow resolution in individual signals), which may be assigned to a mixed contribution of C sp^2 and C sp^3 at lower BE (dark cyan peak) and C bonded to O at higher BE (purple peak). Regarding the fit of the N1s core level region for film **1-PTH**, this shows two components corresponding to the N–CO (pink peak) and *N*-phenyl (brown peak). The latter one is not present in the non-functionalized material **1**. In addition, the fit of the O1s core level for both films is formed by a mixture of two components that could be due to O-(C=O)–Ar at lower BE (dark cyan peak) and O–(C=O)–Ar at higher BE (pink peak), the latter one for film **1-PTH** being broader probably due to the increased number of free carboxylic groups present due to truncation. The same fact was observed in the IR spectra (see above, Fig. 3).

Interestingly, sample **1-PTH** presented broader signals than **1** which could be a result of the disorder introduced during the monomer truncation. In addition, N1s and S2p fit intensities for **1-PTH** material indicated a 4 : 1 ratio of nitrogen and sulfur atoms, which can translate into a functionalization of 20%. This degree of functionalization agrees with that determined from the results of elemental analysis (see the ESI†), which indicated that a functionalization of about 23% had been obtained, as previously indicated by EDX analysis.

Finally, considering that the synthesized materials will be used in heterogeneous photoredox reactions (see below), we carried out the acquisition of their absorption and emission spectra (Fig. 7). The UV-visible absorbance spectrum for the non-functionalized film **1** has negligible light absorption in the UV-vis range (Fig. 7a). However, we observed a strong absorption band at 350 nm for film **1-PTH**, which could be assigned to a n–π^* transition,[11] due to the PTH grafted to the material network (Fig. 7c). Moreover, the photoluminescence analysis for film **1-PTH** showed an intense emission band with a maximum at 450 nm and another smaller emission band at 520 nm when the sample is excited at 350 nm (Fig. 7d). Finally, the band gap value (E_g) between valence and conduction bands of **1-PTH** was calculated by the Tauc plot method, analysing the linear relationship between $(Ahv)^{1/2}$ and photon energy (hv) (Fig. 7c). The E_g values are obtained from the intercept of the extrapolation of the linear branch with the baseline (background). The

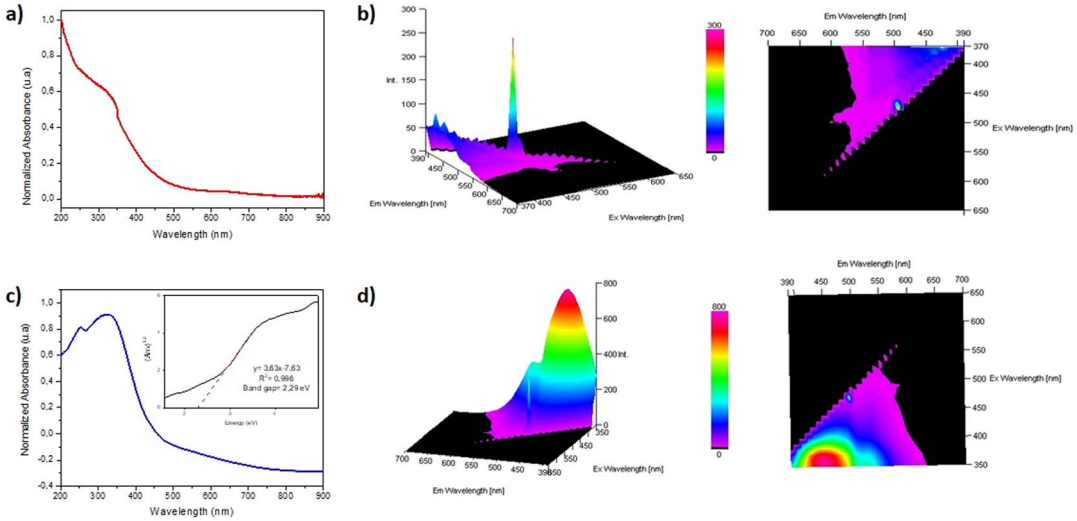

Fig. 7 UV-vis absorption and emission spectroscopy results. Top panels: (a) UV-vis absorption spectra and (b) emission photoluminescence (PL) map for film **1**. Bottom panels: (c) UV-vis absorption spectra and Kubelka–Munk transformed absorption and Tauc plot data and (d) emission photoluminescence (PL) map for film **1-PTH**.

functionalized material **1-PTH** has a band gap value of 2.29 eV due to the phenothiazine grafted over the material network.

Photocatalytic activity

To test the photocatalytic activity of the functionalized film **1-PTH**, we chose the aerobic sulfoxidation[12] and the debromination reactions,[12a,13] which have been observed in related systems using organic solvents.

First, we carried out the synthesis of sulfoxides by the oxidation of thioethers[14] in the presence of oxygen. We began our studies under solvent free conditions obtaining moderate conversions and the formation of random mixtures of thioether/sulfoxide/sulfone when the starting thioether were liquids. Therefore, we carried out the reactions using a small amount of a green solvent such as methanol (200 μL for 0.1 mmol of **8**). Under these conditions, we achieved the corresponding sulfoxides **9** in moderate to good yields from thioethers **8** without the formation of sulfone (Scheme 5). Thus, the oxidation reactions worked well with methylphenylthioether (**8a**) and 2-(methylsulfinyl)naphthalene (**8d**) obtaining high yields. The same results were achieved with sulphides bearing an electron-rich group **8b** and **8c** (72 and 84% yields, respectively). The use of thioether with an electron-withdrawing group at the aromatic ring (**9e** and **9f**) reached sulfoxides in moderate yields. The dialkylsulfide **8g** also underwent oxidation to sulfoxide in excellent conversion without detecting the overoxidation product. Unfortunately, attempts at oxidation of diphenylsulfide were unsuccessful, resulting in only a slight conversion to sulfoxide. This fact could be explained because it is well-known that diphenyl sulfide is better oxidized by radical anion oxygen than by singlet oxygen.[15] In this case, singlet oxygen is the predominant species in the sulfur oxidation reaction.

To determine that the presence of PTH at the film was what allowed this transformation, we studied this aerobic oxidation

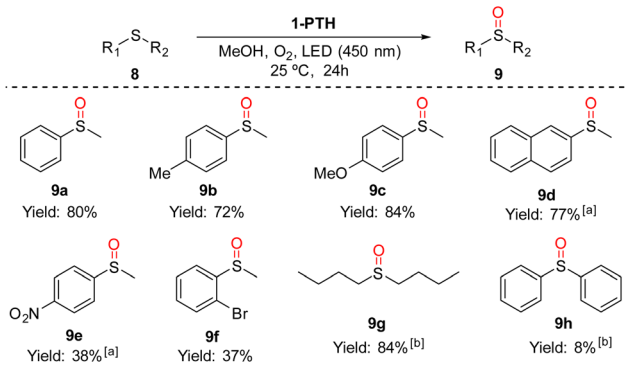

Scheme 5 Reaction conditions: sulphide **8** (0.1 mmol), film **1-PTH** (0.6 mg) in methanol (200 μL) under an oxygen atmosphere was irradiated under 450 nm light for 24 h at rt. Isolated yields are obtained after purification by column chromatography. (a) 400 μL of methanol were used. (b) Yield determined by ^{1}H NMR using 1,3,5-trimethoxybenzene as the internal standard.

with the unfunctionalized film **1**, and very low conversion (10%) with the very reactive thioether **8b** was obtained. This result shows that the pristine film **1** has no photocatalytic capacity.

Finally, and considering the reducing photoredox character of the PTH moiety (E^{o} ($PTH^{\bullet+}$/PTH*) = −2.1 V *vs.* SCE), in order to expand the versatility of the hybrid truncated polymer **1-PTH**, we tested its ability in typical photoreduction reactions. To our delight, film **1-PTH** demonstrated reducing ability in the photochemical dehalogenation of aromatic compounds to their corresponding reduced products **11**. Indeed, substrates **10a** and **10b**, bearing a nitrile and an ester group, respectively, could be efficiently reduced by catalyst **1-PTH** in 100 and 79% conversions, respectively (Scheme 6). However, the bromo derivative **10c**, which presents a ketone group, gave rise only to a low conversion.

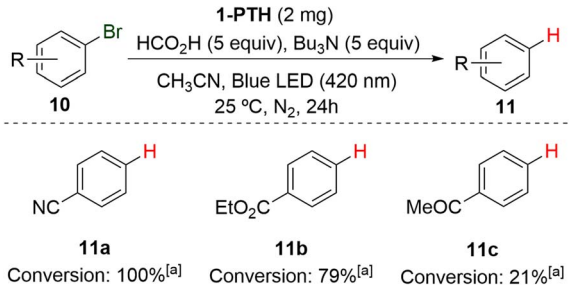

Scheme 6 Use of 1-PTH in the reduction of different aryl bromides. (a) Conversion determined by ^{1}H NMR.

Conclusions

In conclusion, we have introduced the design and synthesis of two novel organic polymer films through the application of a liquid–liquid interfacial amine-acid chloride polymerization technique. Furthermore, one of these films was subjected to *in situ* functionalization *via* the anchoring of *N*-phenyl-phenothiazine using a monomer truncation approach, resulting in the acquisition of photocatalytic capabilities. This photoactive film exhibits intriguing luminescence properties, which were successfully employed in the oxidation of various sulphides to their corresponding sulfoxides as well as for reduction of aryl-halides.

The methodology developed here is presented as a very simple approach for the synthesis of new materials with laminar structures by means of a bottom-up process at a liquid–liquid interface under very mild conditions. In addition, it allows functionalization through a truncation process, which can give access, in an easy manner, to the preparation of new materials that incorporate catalytic units that can be used in heterogeneous phase catalytic processes. New directions in this field could be pursued, such as the use or inclusion of asymmetric monomers, which could lead to asymmetric photocatalytic processes, or the application of these photocatalytic films to water purification.

Author contributions

A. F., V. M. and J. A. conceptualized, designed, and supervised this work. J. V. performed the experiments and the synthesis and characterization of new compounds. A. F. and J. V. prepared the ESI.† M. J. C. and J. A. performed the XPS analysis. A. F. and J. A. wrote the article. All authors contributed to the discussion of the results.

Conflicts of interest

There are no conflicts to declare.

Acknowledgements

This work was supported by the Spanish Ministry of Science and Innovation (projects PID2021-122299NB-I00, TED2021-130470B-I00, and TED2021-129999B-C32), "Comunidad de Madrid" for European Structural Funds (S2018/NMT-4367) and proyectos sinérgicos I+D (Y2020/NMT-6469).

Notes and references

1 (*a*) H. R. Abuzeid, A. F. M. El-Mahdy and S.-W. Kuo, *Giant*, 2021, **6**, 100054; (*b*) C. S. Diercks and O. M. Yaghi, *Science*, 2017, **355**, eaal1585; (*c*) N. Huang, P. Wang and D. Jiang, *Nat. Rev. Mater.*, 2016, **1**, 16068; (*d*) P. J. Waller, F. Gándara and O. M. Yaghi, *Acc. Chem. Res.*, 2015, **48**, 3053; (*e*) J. W. Colson and W. R. Dichtel, *Nat. Chem.*, 2013, **5**, 453; (*f*) J. Sakamoto, J. van Heijst, O. Lukin and A. D. Schlüter, *Angew. Chem., Int. Ed.*, 2009, **48**, 1030.

2 (*a*) T. Zhang and Y. Zhao, Interfacial Synthesis of 2D COF Thin Films, in *Covalent Organic Frameworks*, ed. Y. Gao and F. Lu, IntechOpen, 2023; (*b*) B. Zhang, X. Song, Y. Li, Y. Li, Z. Peng, L. Ye and L. Chen, *Chem. Commun.*, 2020, **56**, 3253; (*c*) H. Wang, Z. Zeng, P. Xu, L. Li, G. Zeng, R. Xiao, Z. Tang, D. Huang, L. Tang, C. Lai, D. Jiang, Y. Liu, H. Yi, L. Qin, S. Ye, X. Rena and W. Tanga, *Chem. Soc. Rev.*, 2019, **48**, 488.

3 For liquid-liquid, see: (*a*) B. Song, L. Zhang, J. Sun, J. W. Y. Lam and B. Z. Tang, *Angew. Chem., Int. Ed.*, 2023, **62**, e202302543; (*b*) D. Yadav, A. Kumar, J. Y. Kim, N.-J. Park and J.-O. Baeg, *J. Mater. Chem. A*, 2021, **9**, 9573; (*c*) J. Liu, S. Wang, T. Huang, P. Manchanda, E. Abou-Hamad and S. P. Nunes, *Sci. Adv.*, 2020, **6**, eabb3188; (*d*) C. Li, Y. Wang, Y. Zou, X. Zhang, H. Dong and W. Hu, *Angew. Chem., Int. Ed.*, 2020, **59**, 9403; (*e*) H.-L. Qian, C.-X. Yang and X.-P. Yan, *Nat. Commun.*, 2016, **7**, 12104, for solid-vapor, see: (*f*) N. A. Khan, R. Zhang, X. Wang, L. Cao, C. S. Azad, C. Fan, J. Yuan, M. Long, H. Wu, M. A. Olson and Z. Jiang, *Nat. Commun.*, 2022, **13**, 3169, for liquid–air, see: (*g*) M. F. Pantano, E. Missale, L. Gazzato, R. Pilot, F. Sedona, G. Speranza and M. Frasconi, *Mater. Today Chem.*, 2022, **26**, 101007.

4 (*a*) Z. Zhuang, H. Shi, J. Kang and D. Liu, *Mater. Today Chem.*, 2021, **22**, 100573; (*b*) K. Geng, T. He, R. Liu, S. Dalapati, K. T. Tan, Z. Li, S. Tao, Y. Gong, Q. Jiang and D. Jiang, *Chem. Rev.*, 2020, **120**, 8814; (*c*) J. L. Segura, M. J. Mancheño and F. Zamora, *Chem. Soc. Rev.*, 2016, **45**, 5635; (*d*) S.-Y. Dinga and W. Wang, *Chem. Soc. Rev.*, 2013, **42**, 548; (*e*) X. Feng, X. Dinga and D. Jiang, *Chem. Soc. Rev.*, 2012, **41**, 6010.

5 (*a*) R. Freund, O. Zaremba, G. Arnauts, R. Ameloot, G. Skorupskii, M. Dincă, A. Bavykina, J. Gascon, A. Ejsmont, J. Goscianska, M. Kalmutzki, U. Lächelt, E. Ploetz, C. S. Diercks and S. Wuttke, *Angew. Chem., Int. Ed.*, 2021, **60**, 23975; (*b*) X. Zhao, P. Pachfule and A. Thomas, *Chem. Soc. Rev.*, 2021, **50**, 6871.

6 A. López-Magano, A. E. Platero-Prats, S. Cabrera, R. Mas-Ballesté and J. Alemán, *Appl. Catal., B*, 2020, **272**, 119027.

7 For a review of defects in COF structures, see:S. Daliran, M. Blanco, A. Dhakshinamoorthy, A. R. Oveisi, J. Alemán and H. García, *Adv. Funct. Mater.*, 2024, **34**, 2312912.

8 (*a*) F. Speck, D. Rombach and H.-A. Wagenknecht, *Beilstein J. Org. Chem.*, 2019, **15**, 52; (*b*) E. H. Discekici, N. J. Treat, S. O. Poelma, K. M. Mattson, Z. M. Hudson, Y. Luo, C. J. Hawker and J. Read de Alaniz, *Chem. Commun.*, 2015, **51**, 11705.

9 N. J. Treat, H. Sprafke, J. W. Kramer, P. G. Clark, B. E. Barton, J. Read de Alaniz, B. P. Fors and C. J. Hawker, *J. Am. Chem. Soc.*, 2014, **136**, 16096.

10 D. González-Muñoz, A. Gómez-Avilés, C. B. Molina, J. Bedia, C. Belver, J. Alemán and S. Cabrera, *J. Mater. Sci. Technol.*, 2022, **103**, 134.

11 L. Piñero, X. Calderón, J. Rodríguez, I. Nieves, R. Arce, C. García and R. Oyola, *J. Photochem. Photobiol. A*, 2008, **198**, 85.

12 (*a*) A. López-Magano, X. Solans-Monfort, N. Salaverri, L. Marzo, R. Mas-Ballesté and J. Alemán, *Sol. RRL*, 2024, **8**, 2300768; (*b*) A. López-Magano, A. Jiménez-Almarza, J. Alemán and R. Mas-Ballesté, *Catalysts*, 2020, **10**, 720; (*c*) A. Jiménez-Almarza, A. López-Magano, L. Marzo, S. Cabrera, R. Mas-Ballesté and J. Alemán, *ChemCatChem*, 2019, **11**, 4916.

13 A. López-Magano, N. Salaverri, L. Marzo, R. Mas-Ballesté and J. Alemán, *Appl. Catal., B*, 2022, **317**, 121791.

14 For other materials with sulfur, see: (*a*) Q. Zhang, Q. Huang, S.-M. Hao, S. Deng, Q. He, Z. Lin and Y. Yang, *Adv. Sci.*, 2022, **9**, 2103798; (*b*) C. Han, T. Zhang, J. Li, B. Li and Z. Lin, *Nano Energy*, 2020, **77**, 105165; (*c*) Y. Yan, P. Zhang, Z. Qu, M. Tong, S. Zhao, Z. Li, M. Liu and Z. Lin, *Nano Lett.*, 2020, **20**, 7662; (*d*) M. Liu, D. Zhou, Y.-B. He, Y. Fu, X. Qin, C. Miao, H. Du, B. Li, Q.-H. Yang, Z. Lin, T. S. Zhao and F. Kang, *Nano Energy*, 2016, **22**, 278.

15 S. M. Bonesi, I. Manet, M. Freccero, M. Fagnoni and A. Albini, *Chem.–Eur. J.*, 2006, **12**, 4844.